Available online at www.sciencedirect.com
SCIENCE DIRECT®
International Journal of Heat and Mass Transfer 48 (2005) 1–14
International Journal of HEAT and MASS TRANSFER
www.elsevier.com/locate/ijhmt

Experimental and numerical characterization of the transverse dispersion at the exit of a short ceramic foam inside a pipe

J.C.F. Pereira [a,*], I. Malico [a,b], T.C. Hayashi [a], J. Raposo [a]

[a] Department of Mechanical Engineering, Instituto Superior Técnico, Av. Rovisco Pais, 1049-001 Lisbon, Portugal
[b] Department of Physics, Universidade de Évora, Av. Romão Ramalho, 59, 7000-671 Évora, Portugal

Received 6 October 2003; received in revised form 17 August 2004

Abstract

The paper theoretically and numerically describes and experimentally studies transverse dispersion of a passive tracer in highly porous ceramic foams of different pore sizes. The pore Reynolds numbers range from 10 to 300. Digital images of the dispersion patterns were recorded and an approximate transverse dispersion coefficient was determined. Numerical solutions of the steady fluid flow and scalar concentrations confirm that the transverse dispersion coefficient models, based on the assumption of dominance of mechanical dispersion and on the linear dependence of the transverse dispersion model on *ud*, are able to predict satisfactorily the dispersion of a tracer for the range of Reynolds numbers considered. An alternative derivation of this linear dependence based on the closure of the volume averaged scalar transport equation is also presented. The influence of the length of the porous media in the stream direction on transversal and longitudinal dispersion is consistent with findings for packed beds at much lower Peclet and Reynolds numbers.

1. Introduction

Flow in porous media is of interdisciplinary interest and traditionally of special relevance to hydrology, petroleum and chemical engineering. Recently, porous ceramic foams, with porosities greater than 85%, or other highly porous materials, such as metal wires and metal foils, have been incorporated in several energy equipments, such as combustors, catalytic exhausters, filters, heat-exchangers, see e.g. Howell et al. [1] and Trimis and Durst [2]. Most of these applications use ceramic foams in the pore size range from 10 to 60 ppi (pores per inch). Consequently, there is research interest in porous media flows at high pore Reynolds numbers, $Re_d = O(10^2)$, and high porosity media, as well as in dodecahedron pore geometric structures typical of ceramic foams.

Scalar dispersion in porous media is assumed to be Fickian at sufficiently large characteristic scales and hence, the governing macroscopic equation has the same form of the transport convection–diffusion equation in which the dispersion coefficients are obtained from correlations or models. There have been many experimental measurements of scalar dispersion in packed beds, see e.g. Pfannkuch [3], Harleman and Rumer [4], Fried and Combarnous [5] and a review of longitudinal and lateral dispersion measurements was presented by Han et al. [6], showing that transverse dispersion grows linearly with Peclet number for $Pe > 1$. Common to the majority of the experiments are the low Reynolds

* Corresponding author. Fax: +351 21 849 52 41.
E-mail address: jose@navier.ist.utl.pt (J.C.F. Pereira).

0017-9310/$ - see front matter © 2004 Elsevier Ltd. All rights reserved.
doi:10.1016/j.ijheatmasstransfer.2004.08.001

Nomenclature

a	particle radius [m]
a_{sf}	area of interface between solid and fluid per unit volume of porous medium [m^{-1}]
c	solute concentration [kg/m^3]
$\hat{c}$	fluctuation of solute concentration [kg/m^3]
C_{ij}	auto covariance matrix of solute particle velocity [$(m/s)^2$]
C_D	drag coefficient
C_E	Ergun coefficient
C_1	coefficient, defined in Eq. (22)
C_2	coefficient, defined in Eq. (16)
D	effective dispersion coefficient [m^2/s]
$\mathbf{D}$	hydrodynamic dispersion tensor [m^2/s]
$\mathbf{D}^*$	total dispersion tensor [m^2/s]
D_m	molecular diffusion coefficient of the solute in the fluid [m^2/s]
D_L	longitudinal component of the total dispersion tensor [m^2/s]
D_T	transverse component of the total dispersion tensor [m^2/s]
d	pore diameter [m]
d_f	fiber diameter [m]
F_i	convective flux at face i of a control volume [$(kg/m^2 s)(m/s)$]
K	permeability of porous medium [m^2]
K_M	kinetic energy per unit mass due to average motion [m^2/s^2]
k_D	kinetic energy per unit mass due to dispersion [m^2/s^2]
L	sample length [m]
M	mass of solute [kg]
$\dot{m}_i$	mass flux at a face i of a control volume [$kg/m^2 s$]
P	pressure [N/m^2]
P_D	production rate of dispersion kinetic energy [m^2/s^3]
Pe	Peclet number based on pore diameter, ud/D_m, or based on particle radius, ua/D_m
$\mathbf{r}$	body force term, in Eq. (5)
R_{is}	radius of incense stick [m]
Re_d	Reynolds number based on pore diameter, ud/ν_f
t	time [s]
u	filtration velocity [m/s]
$\mathbf{v}$	velocity vector [m/s]
$\hat{\mathbf{v}}$	fluctuation velocity vector [m/s]
v_i	component of velocity vector in direction i [m/s]
x,	horizontal (longitudinal) spatial coordinate [m]
x_i	spatial coordinate in direction i [m]
y	vertical spatial coordinate [m]
z	horizontal (transverse) spatial coordinate [m]

Greek symbols

Φ	dissipation rate of dispersion kinetic energy [m^2/s^3]
ε	porosity of porous medium
ϕ	solid volume fraction ($\phi = 1 - \varepsilon$)
γ^*	longitudinal dispersivity [m]
μ_f	dynamic viscosity of fluid [kg/ms]
ν_f	kinematic viscosity of fluid [m^2/s]
ρ_f	density of fluid [kg/m^3]
σ_{ij}^2	covariance matrix of solute particles displacements [m^2]
$\boldsymbol{\tau}$	tortuosity tensor; stress tensor [N/m^2]
ζ	weighting factor used to avoid oscillation in the numerical method

Subscripts

d	pore diameter
T	transverse
L	longitudinal
DL	computational domain length
x	component in direction x
y	component in direction y
z	component in direction z

Superscripts

CDS	central differences approximation
UDS	upwind differences scheme
f	fluid phase
s	solid phase

Others

$\langle\ \rangle$	denotes the local volume average of a quantity, see the Appendix for definition
$\langle\ \rangle^\alpha$	denotes the local intrinsic α-phase average of a quantity, see the Appendix for definition

numbers for which the flow is steady and well described by Stokes theory.

Several models for dispersion in porous media have been developed to express the dependency of the dispersion coefficients on the pore structure. Brenner [7] developed a theory for determining the transport properties in spatially periodic porous media in the presence of convection and showed that, for the long-time limit,

the mean-square displacement of particles grows linearly with time. Carbonell and Whitaker [8] and Quintard and Whitaker [9] developed a closure strategy for the volume averaging form of the convection–diffusion equation in which the macroscopic dispersion coefficient is calculated by solving a closure problem on a unit cell. Several calculations were carried out for two-dimensional spatially periodic porous media, see e.g. Kuwahara et al. [10], Souto and Moyne [11] and Hsiao and Advani [12]. The general theory formulated is based on volume averaging and requires that the pore spatial structure and periodicity be estimated by means of approximate models in order to evaluate the elements of the dispersion and tortuosity tensors. At high Peclet numbers, Koch et al. [13] showed that the mechanism of dispersion in ordered (periodic) and disordered porous media differs qualitatively due to the stochastic fluid velocity field in disordered media that is independent of the molecular diffusivity. For Stokes flow through an array of spheres, Koch and Brady [14] made a comprehensive analysis of the dispersion long-time limit in disordered porous media. It was shown that, for high Peclet numbers, the randomly distributed solid boundaries induce a stochastic velocity field and the resulting mechanical dispersion is proportional to ua and is independent of molecular diffusion. When the solute is trapped in regions from which it can escape only by molecular diffusion the tracer holdup dispersion is proportional to u^2a^2/D_m. Near the solid surfaces, convection and molecular diffusion influence the solute transport and their type of boundary-layer dispersion grows as $ua\ln(Pe)$. The theoretical fundamentals of scalar dispersion in porous media can be found in e.g. Bear [15], Nield and Bejan [16] and Kaviany [17].

Experiments of transverse scalar dispersion in ceramic foams have been conducted only at very high Peclet numbers and were reported by Benz et al. [18] for $Pe = O(10^4)$ and Hackert et al. [19] for $Pe = O(10^8)$. They concluded that the normalised transverse dispersion coefficient, D_T/ud, depends on pore Reynolds number, Re_d, and on the number of pores per inch. The normalised transverse dispersion coefficient increases up to a pore Reynolds number of about 300 or 400 and assumes a constant value in the range of 0.11–0.16 for higher values of Re_d. Questions arise about the dominant dispersion mechanisms at high pore Reynolds numbers and if the dispersion becomes non-Fickian at so high Peclet numbers, see e.g. Lowe and Frenkel [20]. Several calculations of the dispersion in packed beds of spheres have been performed with Lattice–Boltzman, see e.g. Hill and Koch [21], allowing for the identification of transitions from steady to periodic and chaotic dynamics occurring at particle Reynolds number approximately equal to 30. Although there are several turbulence models proposed for calculating turbulent flow in porous media, see e.g. Masuoka and Takatsu [22] and Antohe and Lage [23], there is a lack of complete understanding either about the time and length scales involved and of the occurrence, in the pores, of the "turbulent flow characteristics" or about the equations modeling closures, see e.g. Travkin and Catton [24] and the review of Nield [25].

The main objective of the present work is twofold. Firstly, experimental measurements of the transverse dispersion coefficient, D_T, are reported for flows through short Al_2O_3 ceramic foams with 10, 20 and 60 ppi placed inside a pipe. The present experiments are compared with measurements reported in the literature and with theoretical expressions aiming to deepen the understanding of scalar dispersion in ceramic foams in the range of $10 \leqslant Re_d \leqslant 300$. Secondly, axisymmetric pipe flow calculations are presented in a computational domain that starts upstream of the foam and extends up to a half pipe diameter downstream. The calculation of the transverse dispersion coefficient follows the same procedure used in the experimental procedure and aim to investigate closure models for scalar dispersion coefficients. A dispersion model is derived based on the volume averaging closure of the scalar transport equation.

In the next section of this paper the experimental procedure is described and a comparison between the experimental data obtained in this and other experiments is made. This is followed by a description of the numerical model as well as by a discussion on the predictions, which are compared to the experimental results. The paper ends with summary conclusions.

2. Test section and experimental technique

A schematic drawing of the experimental arrangement is shown in Fig. 1. Air enters a Perspex pipe with 84 mm diameter, which serves as a mount for the test section pipe. It is then guided into the 200 mm long test section pipe through a 20 ppi ceramic foam, which also holds a smoke source incense stick. The porous sample, with an 84 mm diameter and 50 mm long and, is placed in the top of the test section pipe. A laser light sheet, 5 W Ion-Ar, illuminates the exit smoke pattern.

Three ceramic foams made of Al_2O_3 with 10, 20 and 60 ppi were used. The average pore diameters are estimated according to Hackert et al. [19] as being equal to twice the ppi fraction, which gives 5.1, 2.6 and 0.85 mm pore diameters, respectively. The experimental setup is similar to the one proposed by Hackert et al. [19]. In both cases, the foam specimens used are 50 mm long. However, in the present work, the foam specimens have a diameter equal to 84 mm, while those described in [19] had 49 mm in diameter.

The dispersion coefficient, D, defined as the tracer dispersion coefficient in a frame of reference moving with the mean flow velocity, can be calculated from

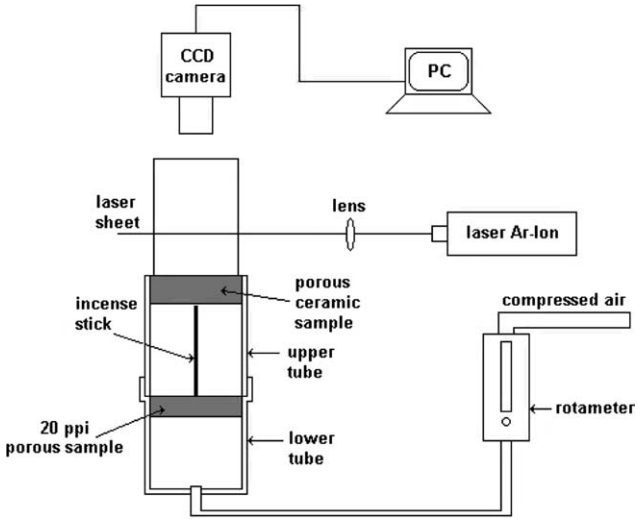

Fig. 1. Schematic drawing of the experimental setup.

the time dependent behaviour of the dispersion tensor, see e.g. Maier et al. [26]:

$$D_{ij}(t) = \frac{1}{2}\frac{\mathrm{d}}{\mathrm{d}t}[\sigma_{ij}^2(t)] = \int_0^t C_{ij}(t')\,\mathrm{d}t' \tag{1}$$

where the tensor $\sigma_{ij}^2 = \langle [x_i(t) - \langle x_i(t)\rangle][x_j(t) - \langle x_j(t)\rangle]\rangle$ is the covariance matrix of solute particle displacements and the tensor $C_{ij}(t) = \langle [v_i(t) - \langle v_i\rangle][v_j(0) - \langle v_j\rangle]\rangle$ is the auto covariance matrix of solute particle velocity in the pores. If $\mathrm{d}[\sigma_{ij}^2(t)]/\mathrm{d}t$ is constant, then Fick's law is appropriate to describe dispersion and this derivative is equivalent to twice the dispersion tensor of the advection–diffusion equation [15]. In the present work, only the measurements of the dispersion rate in the transverse direction were performed, by means of the calculation of the variance (σ^2) of the solute concentrations, following the procedure outlined in [19].

Digital images of the resulting smoke distribution profile at the outlet plane of the porous ceramic sample were taken using a CCD camera linked to a frame grabber video card with a 640×480 pixels resolution that processes and stores in a computer the digitised images with 256 grey levels. In Fig. 2(a) an example of such images is presented. The approximate transverse dispersion coefficient was evaluated from the digital images by assuming that the tracer intensity at each pixel is correlated with the tracer concentration and that the dispersion of individual tracer particles approaches a Gaussian distribution in the continuum limit.

The analytical solution of the three-dimensional transport of an amount of mass M injected at a point source at time $t = 0$, is given by Eq. (2).

$$c(x,y,z,t) = \frac{M}{8\varepsilon(\pi t)^{1.5}\sqrt{D_x D_y D_z}} \times \exp\left[-\frac{(x-ut)^2}{4D_x t} - \frac{y^2}{4D_y t} - \frac{z^2}{4D_z t}\right] \tag{2}$$

Assuming that the concentration profile is Gaussian, the dispersion coefficient is given by $4tD_\mathrm{T} = 2\sigma_y^2$. The variation of the average transverse dispersion coefficient between two moments in time t_1 and $t_2 = t_1 + \Delta t$ is $\Delta\sigma^2 = \sigma_2^2 - \sigma_1^2 = 2D_\mathrm{T}(t_2 - t_1)$. For steady flow, time can be replaced by downstream distance $\Delta x = \Delta t \cdot u$, or $L = u \cdot \Delta t$, yielding the transverse dispersion to be equal to Eq. (3).

$$D_\mathrm{T} = \frac{u}{2}\frac{\Delta\sigma^2}{L} \tag{3}$$

The procedure to calculate $\Delta\sigma^2 = \sigma_2^2 - \sigma_1^2$ consists in comparing the evolution of the variances of the images intensity at the inlet and outlet planes of the ceramic foam. The variance is calculated as the mean value of the variances along the two orthogonal coordinate directions centered at the image mass centre and evaluated from five stored images. Fig. 2(b) shows a typical image intensity profile, whose similarity to the scalar concentration profile is used to calculate the dispersion coefficient. Very near the foam outlet the flow is characterised by pore-like discrete three-dimensional micro-jets that are very stable in the range of Reynolds numbers investigated. The peak values presented in Fig. 2(b) denote the signatures of those micro-jets. After perturbing the outlet flow between two consecutive images there was virtually no difference in the two images intensities. This explains the very low scatter observed in the averaged data from 5 or 10 images, which was less than

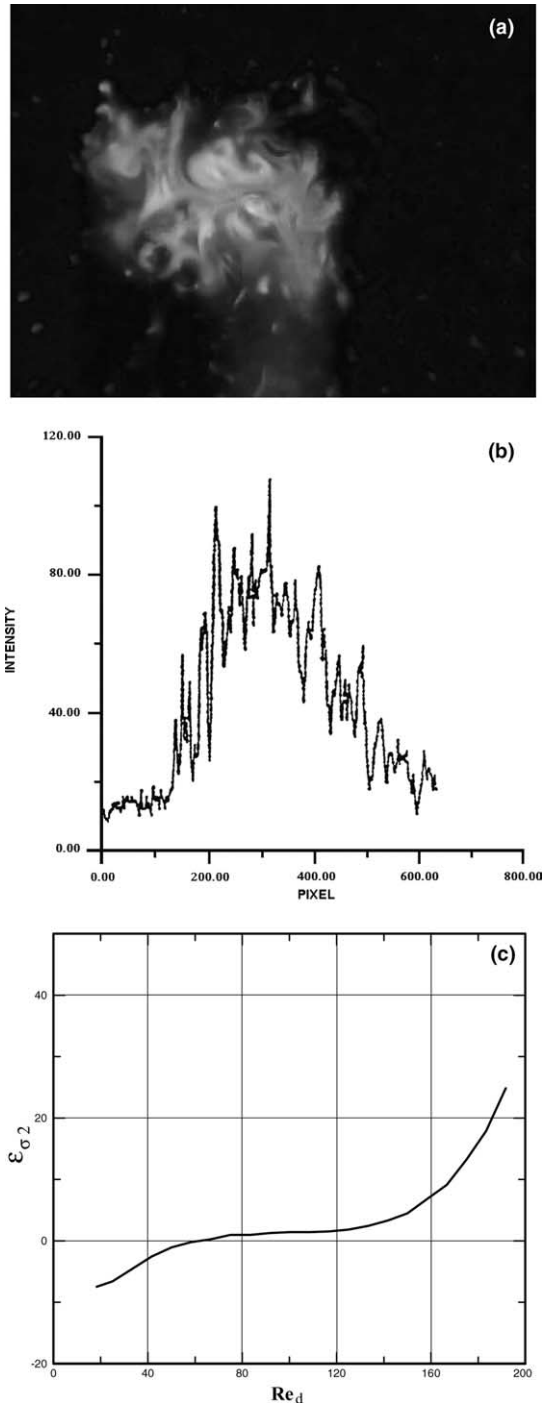

Fig. 2. (a) Smoke image at the outlet of the ceramic foam (20 ppi foam, $Re_d = 47.5$); (b) Image intensity profile (20 ppi foam, $Re_d = 40$); (c) Relative error as function of the pore Reynolds number for a 20 ppi foam.

1% of the value of the variance corresponding to each image. The accuracy of the variance values is dependent on the image signal to noise ratio, which deteriorates with the increase of the pore Reynolds number. The variance was measured only up to the pore Reynolds number that produced an amplitude of the image intensity at least one order of magnitude higher than the background intensity. There are several error sources in the method used to calculate the transversal dispersion: (i) the smoke production source steadiness between the captured images at inlet and outlet of the porous medium. Monitoring the diameters of the incense sticks and constantly testing the burning velocity allowed to conclude that this error source is negligible (because the change in the variance of the image intensity at the inlet was negligible compared to the variance of the image intensity at the outlet of the ceramic foam); (ii) the measured intensity profiles have deviations from Gaussian distributions, consequently the calculations of the first and second moments deviate from those of the Gaussian distribution; and (iii) the signal to noise ratio decreases with the increase of Reynolds number, limiting the application of the technique.

The calibration of the distance from the physical space to the digital image in pixels only induces an estimated error lower than 0.1% of the distance. In order to conduct an error estimation of Eq. (3), the measured moments of the intensity distribution were compared with those of the best fit of a Gaussian distribution. Fig. 2(c) shows the relative error as a function of the pore Reynolds number for the 20 ppi foam. Below $Re_d \approx 40$, there is an underestimation of around 10%, while for $Re_d > 150$, the error grows very rapidly reaching 35% at $Re_d = 300$. Similar results were obtained for 10 and 60 ppi foams and the results that will be presented correspond to Reynolds numbers where the estimated error is smaller than 20%. Confirmation of the results, either by experiments repetition or by rotating the porous medium, showed that the relative error was always smaller than 20%.

3. Numerical model

The local volume averaged forms of the differential balance laws (continuity, momentum and scalar concentrations) for an incompressible, steady flow through a porous medium can be established, see e.g. Vafai and Tien [27] and Carbonell and Whitaker [8], as:

$$\nabla \cdot \langle \mathbf{v} \rangle = 0 \tag{4}$$

$$\langle (\mathbf{v} \cdot \nabla)\mathbf{v} \rangle = -\frac{1}{\rho_f} \nabla \langle P \rangle + \nu_f \nabla^2 \langle \mathbf{v} \rangle + \frac{\mathbf{r}}{\rho_f} \tag{5}$$

$$\frac{1}{\varepsilon} \langle \mathbf{v} \rangle \cdot \nabla \langle c \rangle = -\mathbf{D}^* \cdot \nabla^2 \langle c \rangle \tag{6}$$

In Eq. (5), **r** stands for the body force term, which is caused by the micropore structure and measures the resistance imposed by the solid matrix to the fluid flow:

$$\mathbf{r} = -\frac{\mu_f}{K}\langle \mathbf{v} \rangle - \frac{C_E}{K^{1/2}}\rho \langle \mathbf{v} \rangle \mathbf{v} \tag{7}$$

where C_E stands for the Ergun coefficient.

The total dispersivity tensor $\mathbf{D}^* = D_m[\mathbf{I} + \boldsymbol{\tau}] + \mathbf{D}$, in Eq. (6), receives contribution from molecular diffusion, $D_m\mathbf{I}$, from the tortuosity of the porous media, $D_m\boldsymbol{\tau}$, and from the effect of the velocity field through the dispersion tensor **D**.

Since the scalar dispersion from a point source yields a three-dimensional dispersion pattern, the calculations of the flow upstream, through and downstream of the ceramic foam cylinder inserted in a pipe were axisymmetric. The problem arises of how to model the longitudinal, D_L, and transversal, D_T, components of the tensor $\mathbf{D}^*$. For most cases, the transversal dispersion is at least one order of magnitude smaller than the longitudinal dispersion, which is expressed by $D_L = \gamma^* u + D_m$, the dispersivity, D_L/u, being a characteristic property of the medium. Problem dependent correlations for D_L/u are available, either at column scale or for field applications. The selection of D_L and D_T will be discussed in the next section.

Although the flow problem under consideration could be calculated only by the scalar transport equation with the prescribed velocity field, for generality reasons, the continuity and two momentum equations for axisymmetric flow were solved with the finite volume SIMPLE algorithm [28]. To decrease false diffusion owing to first order upwind schemes, the deferred correction numerical treatment of convection [29] is used. The convective fluxes are approximated by:

$$F_i = [\dot{m}_i v_i^{UDS}]^m + \dot{m}_i[v_i^{CDS} - v_i^{UDS}]^{m-1} \tag{8}$$

where m denotes the iteration level.

The second term on the right-hand side is evaluated using values from the previous iteration, while the firs one is computed using the UDS approximation. On convergence, the UDS contribution cancels out leaving the CDS solution that is free from dissipation errors, but would require a factor $\zeta < 1$ to avoid oscillatory solutions. For the present case $\zeta = 0.85$.

The computational domain consists of an axisymmetric pipe with an 84 mm diameter and a porous cylinder inside. The pipe inlet is located 5 mm upstream of the porous foam, which is 50 mm long, and the outlet is located one half-pipe diameter downstream of the foam. Eqs. (4)–(6) are solved along with the proper boundary condition, which are as follows:

At the inlet ($x = 0$),

$$v_x(0,y) = u; \quad v_y(0,y) = 0; \quad c(0,y) = \begin{cases} 1 & \text{for } y \leqslant R_{is} \\ 0 & \text{for } y > R_{is} \end{cases} \tag{9}$$

At the outlet of the computational domain ($x = x_{DL}$),

$$\frac{\partial c}{\partial x}(x_{DL},y) = \frac{\partial v_x}{\partial x}(x_{DL},y) = \frac{\partial v_y}{\partial x}(x_{DL},y) = 0 \tag{10}$$

At the pipe wall, non-slipping condition and impermeability to the tracer are imposed. The interface conditions between the porous medium and the clear fluid were satisfied due to the use of the control volume face fluxes equality. The normal and the tangential stresses were made continuous through the interface.

4. Results

Effective transverse diffusivity, D_T normalised effective transverse diffusivity, D_T/ud, and transverse dispersivity, D_T/u, are presented in Fig. 3(a), (b) and (c), respectively, as functions of the pore Reynolds number and for different pore sizes. The present experiments are compared with data reported for ceramic foams by other authors. Since the present experimental conditions are similar to those reported by Hackert et al. [19], the data compares satisfactorily and falls inside the maximum 20% relative error estimation that was also reported in that work. The experimental results reported by Benz et al. [18] were obtained at higher pore Reynolds numbers and are consistent with the trend observed in the present measurements. Fig. 3(a) and (b) show a strong dependence of D_T on the pore Reynolds number. The increase in D_T can be attributed to a pure mechanical dispersion process in which the smoke molecular diffusion is not relevant for each of the foams considered.

The data corresponding to the upper limit of the Reynolds number in Fig. 3(a)–(c) is subjected to some controversial interpretation. Hackert et al. [19] as well as Benz et al. [18] suggest that the normalised effective transverse dispersion coefficient, D_T/ud, increases with Reynolds up to about $300 < Re_d < 400$, see Fig. 3(b), and then becomes approximately constant with Re_d owing to turbulent mixing within the pores. The critical Reynolds number for transition to purely turbulent flow in packed beds is in the range of $Re_d \approx 150$ according to Jolls and Hanratty [30] while, for Dybbs and Edwards [31], this transition occurs for $Re_d \approx 300$. For ceramic foams, according to Hall and Hiatt [32], the critical Reynolds number is in the range of $300 \leqslant Re_d \leqslant 400$.

For Stokes flow through a random packed bed of spheres, Koch and Brady [14] derived analytical expressions for the longitudinal and transverse dispersion coefficients. Since the solid phase is not permeable to the tracer, for $Pe \gg 1$, D_L and D_T are given by:

$$\frac{D_L}{D_m} = 1 + \frac{3}{4}Pe + \frac{1}{6}\pi^2 \phi Pe \ln(Pe) \tag{11}$$

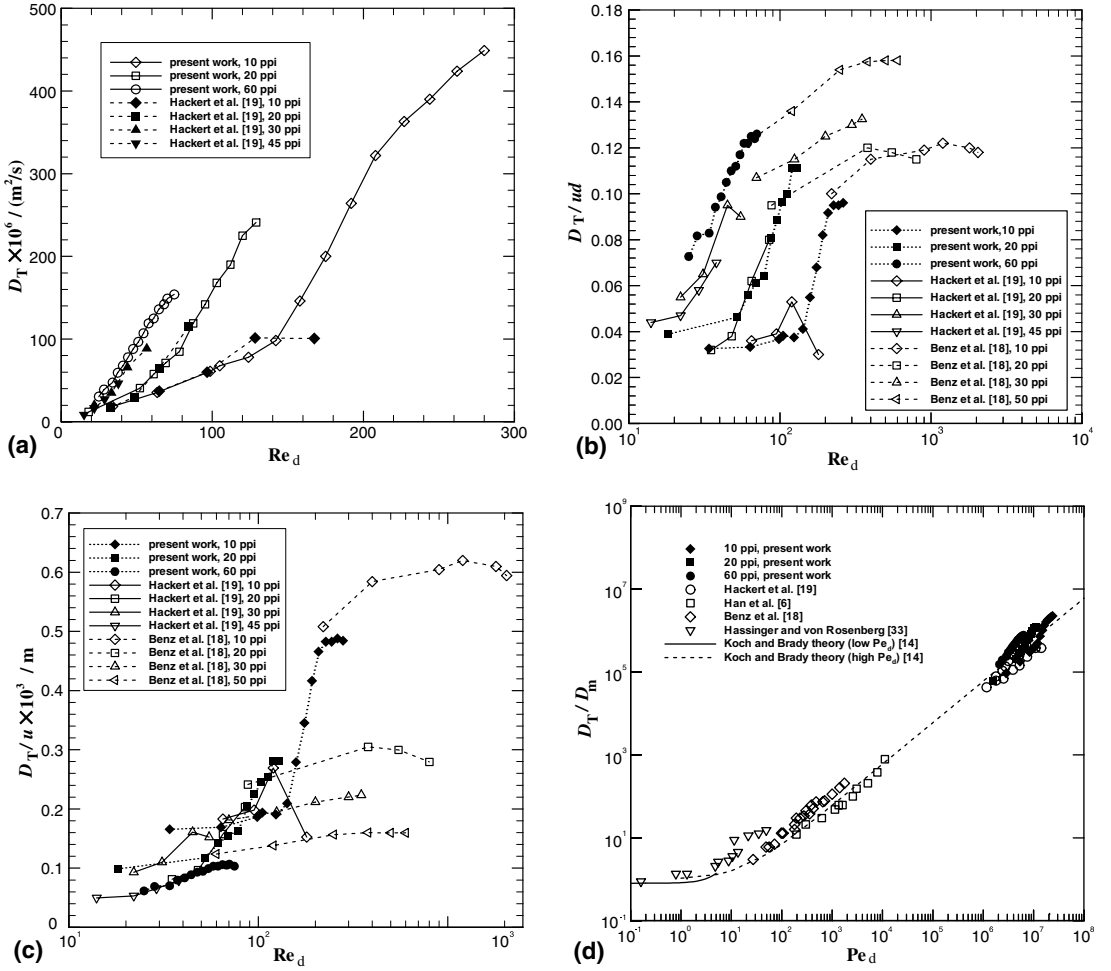

Fig. 3. (a) Effective transverse diffusivity as function of the pore Reynolds number for several ceramic foams; (b) Normalised effective transverse diffusivity as function of the pore Reynolds number for several ceramic foams; (c) Transverse dispersivity as function of the pore Reynolds number for several ceramic foams; (d) Comparison of effective transverse diffusivity measurements with theory.

$$\frac{D_T}{D_m} = 1 + \frac{63}{320}\sqrt{2\phi}Pe \tag{12}$$

In the above equations, the length scale used in the Peclet number is the sphere radius.

A plot of Eq. (12) is shown in Fig. 3(d) together with the present measurements and including also data from low Peclet number flows in fixed beds ([6] and [33], *cit. in* [19]). The length scale used in Eq. (12) for the Peclet number was the pore diameter. In the expressions of Koch and Brady, the Peclet number is based on the sphere radius [14]. They were modelling dispersion in packed beds where the porous medium is composed of particles. This paper reports the modelling of dispersion in ceramic foams, consolidated media, where the characteristic length is the pore diameter. One should note that for ceramic or metal foams, the reported equivalent particle diameter, for a given ppi number, is smaller than the pore diameter [1,34] and consequently Eq. (12), based on an equivalent particle radius length scale, would strongly underpredict the dispersion coefficient. The logarithmic plot shows that the theoretical curve, Eq. (12), is a satisfactory approximation of all the experimental data. Two-dimensional calculations performed using models or correlations of the dispersion coefficients in the scalar transport equation will be reported in the next paragraphs.

According to Eq. (6), one needs to supply both transverse and longitudinal dispersion coefficients to the governing equations. The present experimental method does not allow measuring the longitudinal diffusion coefficient and, to the authors' knowledge, this coefficient is not available for ceramic foams. Therefore, a numerical study was conducted to find out the influence of this

coefficient. The study consisted in assigning the longitudinal and transversal coefficients to the equations and calculating, from the resulting concentration field solution, the transverse diffusivity. The calculation of the transverse diffusivity followed the procedure used in the experiments and expressed in Eq. (3), in which the variance immediately downstream of the foam, σ_2^2, and at the inlet, σ_1^2, were calculated from the predicted concentration profile in the same manner as in the experimental procedure.

In order to assess the influence of the mesh refinement on the predictions, a grid sensitivity study was undertaken. The numerical grid used in the two-dimensional, axisymmetric calculations expands in both axial and radial directions in order to concentrate the grid lines in the zone of main interest for the study of the dispersion of a scalar inside the foam. Three meshes were considered: 53×40, 106×80 and 212×160. Fig. 4 shows the concentration of points in the dispersion region close to the centreline, as well as a detail of the predicted isocontours of concentration of solute in that region. The transverse dispersion coefficients calculated with the finest grid are less than 0.1% smaller than the ones obtained with the 106×80 grid, while the coarsest mesh results are 1% higher, which denotes the independence of the solution on further grid refinement. Therefore, the numerical results presented in this work were obtained with the 106×80 grid.

Recalling from Fig. 3(d) that the theoretical D_T results by Koch and Brady [14], Eq. (12), agree well with the experimental data in the high Reynolds number region, Fig. 5(a) shows that if the scalar transport equation uses D_L and D_T given by Eqs. (11) and (12), respectively, the predicted dispersion coefficients are lower than the value used in the transport equation, the differences being higher for the case of the 10 ppi foam and relatively lower for the 60 ppi foam. These results indicate that, for the short lengths of the foam sam-

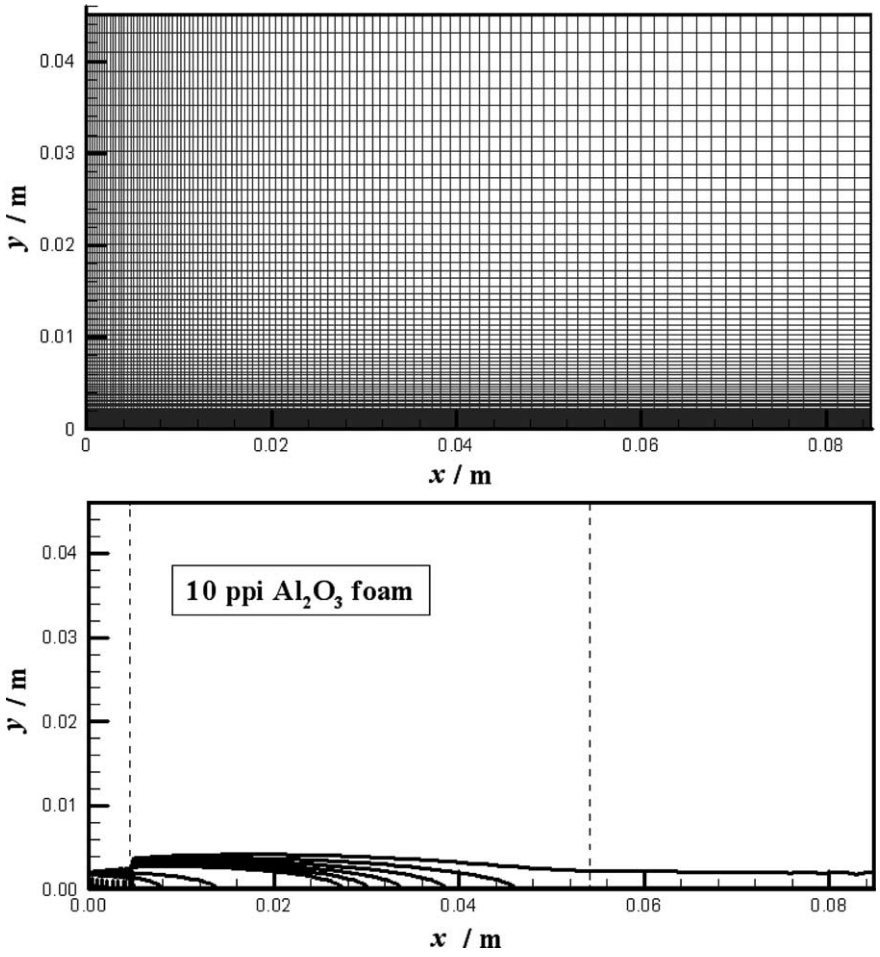

Fig. 4. Calculation domain and mesh used in the computational model. Detail of solute mass fraction isocontours close to the centreline, ranging from 1.0 to 0.1 with a 0.1 increment and from 0.09 to 0.05 with a 0.01 increment (results for 10 ppi foam, $Re_d = 400$).

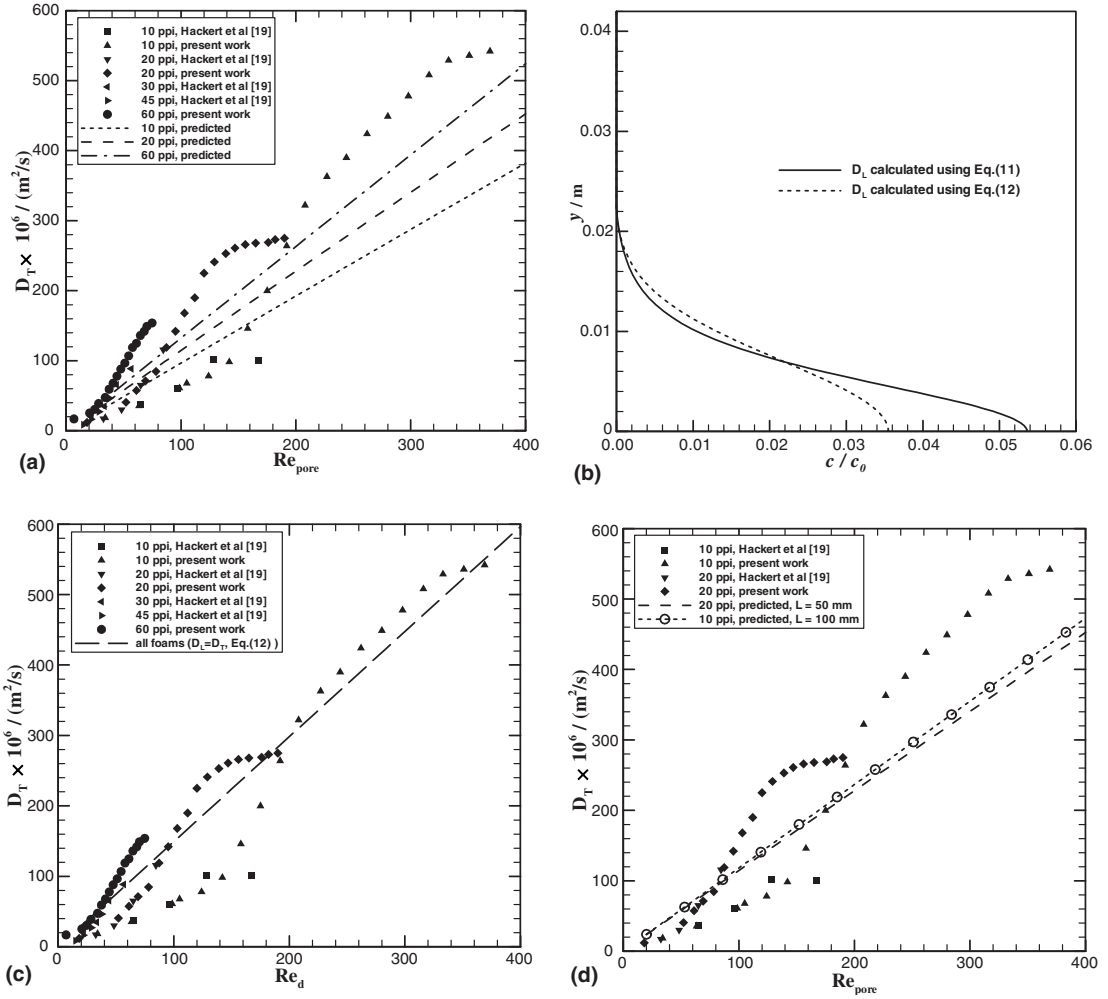

Fig. 5. (a) Comparison of effective transverse diffusivity measurements (filled symbols) and predictions (lines) as function of pore Reynolds number. In all predictions, D_L and D_T were calculated according to Eqs. (11) and (12), respectively, and $L = 50$ mm; (b) Ratio of predicted concentration at the porous sample outlet plane to the initial concentration of solute (10 ppi foam, $Re_d = 400$, $c_0 = 1.0\,kg/m^3$); (c) Comparison of effective transverse diffusivity measurements (filled symbols) and prediction (line) as function of pore Reynolds number. In the calculation, $D_L = D_T$ were calculated according to Eq. (12), and $L = 50$ mm; (d) Comparison of effective transverse diffusivity measurements (filled symbols) and prediction (line) as function of pore Reynolds number. In the predictions, D_L and D_T were calculated according to Eqs. (11) and (12), respectively.

ples used in the present work, the longitudinal dispersion coefficient influences the concentration profile and consequently the prediction of D_T.

In order to evaluate this influence, Fig. 5(b) shows the concentration profile at the foam outlet, for 10 ppi and $L = 50$ mm, obtained using D_L given by Eq. (11) or made equal to D_T which means that the D_L value introduced in the scalar transport equation is of the order of one-tenth of the theoretical value obtained with Eq. (11). Fig. 5(c) shows the D_T values predicted for the decreased D_L case when D_L and D_T used in the scalar transport equation are both calculated with Eq. (12). In this case, the influence of the pore sizes is not observed, and the predicted D_T values present a better agreement with the experimental data.

The strong influence of the D_L value in short foams is in agreement with the study in fixed beds of Han et al. [6], which demonstrates the need to observe a minimum dispersion length to obtain measurements of the longitudinal dispersion coefficients that are not dependent on the position in the packed bed. In this paper, it is also shown that the dispersion length constraint is dependent on the value of the Peclet number. Additionally, Han et al. [6] conclude that one should expect that the transverse diffusivity measured in a transient experiment would be subjected to the same long-time constraint as

the longitudinal diffusivities. Adapting the reasoning of Han et al. [6] in their one-dimensional analysis to the longitudinal direction in this problem, and adopting the pore diameter as the characteristic length scale for flow in ceramic foam, this constraint can be expressed as

$$\frac{L}{d}\frac{\varepsilon}{Pe} \gg 1 \tag{13}$$

confirming that the larger the Peclet number, the larger the required length for constant axial dispersion coefficients to be observed.

It is not possible to extrapolate directly the results from packed beds to ceramic foams, but one should expect that the longitudinal diffusivity would be dependent on L/d, up to the required ratio of foam length to particle or pore diameter in order to treat the longitudinal diffusivity as constant. On the other hand, it was not found that the column length affects the transverse dispersion coefficient. If the critical L/d value is not satisfied, one observes significantly lower values of the coefficients. Han et al. [6] wrote "some of the previous results in the literature indicate that the longitudinal dispersivity depends less strongly on the Peclet number at very high values of Peclet, than at lower values. This has been attributed to turbulence effects. However, a similar phenomenon is observed in this work under laminar flow conditions when the dispersion distances are too short to satisfy the constraint", (Eq. (13)). Fig. 5(d) shows that if the length L of the 10 ppi foam is doubled, the predicted D_T agrees with the predictions obtained for the 20 ppi foam with $L = 50$ mm, because the L/d ratio is the same. Many calculations were performed and the final conclusion is that for foams with $L = 50$ mm one needs to reduce D_L in order to predict a D_T value closer to the one used in the scalar transport equation. Numerical results obtained for different D_L values and for 10, 20 and 60 ppi foams with 50 mm in length, show that to fulfil the requirement of the predicted D_T being equal to the one used in the transport equation, the D_L should be approximately equal to D_T.

5. Discussion

Fig. 5(c) shows predictions of D_T in satisfactory agreement with the experimental data, bearing in mind the scatter in the data. One should take in consideration that the theoretical model of Koch and Brady [14], although for $Pe \gg 1$, was based in the Stokes flow assumption. In addition, the literature reveals that even for isotropic porous media the transverse and longitudinal coefficients are not equal when the medium is so long that constant axial dispersivities are reached. Consequently the previous results, in the range $10 < Re_d < 300$, are also in agreement with the analysis presented by Han et al. [6] about the effect of the packed bed length on the longitudinal dispersion coefficient.

When mechanical dispersion is the dominant mode, the dispersion coefficients are proportional to ud, see e.g. the analysis of five different models of transverse thermal dispersion conducted by Alazmi and Vafai [35]. The same is true for the effective diffusivity of fibrous media, approximated by cylinders, see Koch and Brady [36]. There have been several assumptions to derive this dependence and, in this paper, the authors present one that will be obtained from closure modelling of the volume averaged scalar transport equation.

One can define spatial deviations of the point concentration and fluid velocity in terms of the intrinsic phase average values [8,37] according to $c = \langle c\rangle^f + \hat{c}$ and $\mathbf{v} = \langle \mathbf{v}\rangle^f + \hat{\mathbf{v}}$. It is admitted that, in the solid, $\hat{c} = \langle c\rangle^s = 0$ and $\hat{\mathbf{v}} = \langle \mathbf{v}\rangle^s = 0$. The scalar transport equation as derived by Gray [37] is:

$$\frac{\partial\langle c\rangle}{\partial t} + \frac{1}{\varepsilon}\langle \mathbf{v}\rangle \cdot \nabla\langle c\rangle = \nabla \cdot (\mathbf{D}^* \cdot \nabla\langle c\rangle) \tag{14}$$

where

$$\mathbf{D}^* \cdot \nabla\langle c\rangle = D_m(\nabla\langle c\rangle + \boldsymbol{\tau}) - \langle \hat{c}\hat{\mathbf{v}}\rangle \tag{15}$$

Consequently, the dispersive scalar flux vector is modelled according to gradient type, Fickian law with an unknown dispersion coefficient $\mathbf{D}^*$.

The modelling assumption for the dispersion coefficient made in this study is generally based in dimensional analysis. Since k_D has units m^2/s^2 and D^* units are m^2/s, one may express the dispersion coefficient as:

$$D^* = C_2 k_D^2/\Phi \tag{16}$$

In Eq. (16), Φ stands for the dissipation rate of the "dispersion" kinetic energy and has units m^2/s^3. The equation for k_D is derived in the Appendix. Under equilibrium assumptions, one may simplify the k_D equation by estimating that there is a dominant role of production and dissipation in the energy budget relatively to other transport terms. The production term may be modelled by:

$$P_D = \frac{1}{2} C_D a_{sf} \langle u\rangle^2 \langle u\rangle \tag{17}$$

where a_{sf} denotes the area per unit volume of the porous media, u stands for the filtration velocity and C_D is the drag coefficient.

Bhattacharya et al. [34] and Calmidi and Mahajan [38] provide a model for the estimation of a_{sf} which is based on a representation of the approximate foam structure as an open cell shaped like a dodecahedron, yielding:

$$a_{sf} = \frac{3\pi}{(0.59)^2 d} G(\varepsilon)\frac{d_f}{d} \tag{18}$$

where:

$$\frac{d_f}{d} = 1.18\sqrt{\frac{1-\varepsilon}{3\pi}}\frac{1}{G(\varepsilon)} \tag{19}$$

In Eqs. (18) and (19), the shape function $G(\varepsilon)$ is included to take into account the variation of the struts cross-section with porosity:

$$G = 1 - e^{-(1-\varepsilon)/0.04} \tag{20}$$

Thus, Eq. (18) can be written as:

$$a_{sf} = \frac{H(\varepsilon)}{d} \tag{21}$$

Dimensional analysis shows that scalar dissipation can be evaluated using a prescribed length scale equal to the pore diameter:

$$\Phi = \frac{k_D^{3/2}}{d}C_1 \tag{22}$$

Replacing the value of Φ in Eq. (16) yields:

$$D_T = C_2 \cdot k_D^{1/2} \cdot d \tag{23}$$

The dispersive kinetic energy can be extracted by equating $P_D = \Phi$,

$$\frac{1}{2}C_D u^3 H(\varepsilon) = k_D^{3/2} \cdot C_1 \tag{24}$$

yielding:

$$D_T = \frac{C_2}{C_1^{1/3}}\left[\frac{1}{2}C_D \cdot \frac{3\pi}{0.59^2}1.18\sqrt{\frac{1-\varepsilon}{3\pi}}\right]^{1/3} ud \tag{25}$$

The value of C_D that stands for the bulk drag coefficient is a function of ε [39], and a rough estimation is $C_D \approx 0.5$. For the case under consideration, in Eq. (25) $\varepsilon = 0.87$, which yields $D_T = 0.91\frac{C_2}{C_1^{1/3}}ud$. The determination of the constants is out of the scope of this work, but taking into consideration that $C_1^{1/3}$ should be close to unity and under the assumption that $C_2 \approx 0.1$, the derivation of D_T is very close to the Koch and Brady's result ($D_T = 0.1ud$), and consequently with the measurements. The important remark concerning this discussion is that D_T is a linear function of Peclet for a prescribed ε and as far as C_D is constant in Eq. (25).

The above procedure is not valid for turbulent flow because time was not considered. So, the similarities with turbulent flow analysis are only due to the mathematical decomposition of the point values of the quantities into a mean part and a fluctuation. The described approach is valid as far as the modelling of the production and dissipation of "dispersion" kinetic energy and the equilibrium assumption are physically sound.

6. Conclusions

This paper reports experimental, numerical and theoretical results of transverse dispersion coefficients for flow in the range $10 < Re_d < 300$ within high porosity ceramic foams with 10, 20 and 60 pores per inch. The main results are summarized as follows.

Experiments show a dependence of D_T on the pore Reynolds number. The increase of D_T with Re_d can be attributed to a pure mechanical dispersion process.

Calculation of the transverse dispersion coefficient by means of the theoretical expression by Koch and Brady [14], using the pore diameter as a characteristic length, agrees satisfactorily with the experiments, despite the high Reynolds number considered.

Numerical predictions using D_L and D_T according to Koch and Brady in the scalar transport equation were performed with the aim of recovering the D_T value from the calculated concentration field following the procedure used in the experiments. The predictions show the strong dependence of D_L on the foam length to pore diameter ratio (L/d) and the influence of this dependence in the recovered D_T values. The D_T value for 60 ppi is better predicted than for 10 ppi, because the former has a higher L/d value. For the 60 ppi foam, this value is approximately 60 while the 10 ppi foam has $L/d \cong 10$.

Owing to the short foam length considered, the D_L value introduced in the scalar transport equation was decreased according to the theoretical findings for packed beds, yielding excellent agreement of the D_T values estimated using the expression by Koch and Brady with the ones recovered from the predictions.

For the range of pore Reynolds number considered, dispersion in porous media is mainly due to mechanical dispersion, which results in the dispersion coefficient being proportional to ud. The Koch and Brady's theoretical relationship for D_T is in agreement with the experiments. A derivation for D_T is presented, which is based on the modelling closure of the volume average form of the scalar transport equation. The dispersive scalar flux vector in this equation is modelled from the dispersive kinetic energy and a pore diameter prescribed length scale.

Acknowledgments

This work was partially supported by *Fundação para a Ciência e a Tecnologia* (Lisbon, Portugal, FCT project number PRAXIS/3/3.1/CTAE/1915/95) and by EC project ENK6-CT-2000-00317. T.C. Hayashi would like to thank the *Fundação Coordenação de Aperfeiçoamento de Pessoal de Nível Superior*, CAPES (Brasilia, Brazil) for the Ph.D. fellowship granted.

Appendix A. Derivation of the averaged form of balance equations

The phase average of some quantity ψ_α of the α-phase is defined as:

$$\langle\psi_\alpha\rangle = \frac{1}{V} = \int_{V=V_\alpha+V_\beta} \psi_\alpha \, dV \tag{A.1}$$

In this development, it is assumed that the value of ψ_α is zero in the β-phase. On the other hand, $\langle\psi_\alpha\rangle$ is an average associated with some point in the flow domain. This point is not necessarily in the α-phase, so that $\langle\psi_\alpha\rangle$ is defined for the whole space and may be non-zero in the β-phase.

A second average to consider is the intrinsic phase average, which is computed by finding the integral only over the volume V_α of the α-phase contained in the representative elementary volume V:

$$\langle\psi_\alpha\rangle^\alpha = \frac{1}{V_\alpha}\int_{V_\alpha} \psi_\alpha \, dV \tag{A.2}$$

The two averages are related by

$$\varepsilon_\alpha\langle\psi_\alpha\rangle^\alpha = \langle\psi_\alpha\rangle \tag{A.3}$$

where $\varepsilon_\alpha = V_\alpha/V$. This variable is the porosity of the porous medium if α is the fluid phase.

Another important relationship is the theorem that relates the average of a derivative to the derivative of an average [40]:

$$\langle\nabla\psi_\alpha\rangle = \nabla\langle\psi_\alpha\rangle + \frac{1}{V}\int_{A\alpha\beta} \psi_\alpha \mathbf{n}_\alpha \, dA \tag{A.4}$$

where $A_{\alpha\beta}$ is the area of the α–β interface and $\mathbf{n}_\alpha$ is the outwardly oriented unit vector normal to $A_{\alpha\beta}$.

In what follows, all quantities are defined in the α-phase (fluid) and, for convenience, the subscript will no be longer indicated with velocity, pressure and energy contents. However, it will be indicated along with fluid properties, meaning that these properties are evaluated as intrinsic phase averages and admitted to be constant.

The phase averaged balance equation for kinetic energy (mechanical energy for an isothermal flow) reads [41]:

$$\begin{aligned}&\left\langle\frac{\partial}{\partial t}\left(\frac{v_i v_i}{2}\right)\right\rangle + \left\langle\frac{\partial}{\partial x_j}\left(\frac{v_i v_i}{2}v_j\right)\right\rangle \\ &\quad = -\left\langle\frac{1}{\rho}\frac{\partial(Pv_j)}{\partial x_j}\right\rangle + \left\langle v\frac{\partial}{\partial x_j}\left[\frac{\partial}{\partial x_j}\left(\frac{v_i v_i}{2}\right)\right]\right\rangle \\ &\qquad - \left\langle v\left(\frac{\partial v_i}{\partial x_j}\frac{\partial v_i}{\partial x_j}\right)\right\rangle\end{aligned} \tag{A.5}$$

According to the general transport theorem [40],

$$\left\langle\frac{\partial}{\partial t}\left(\frac{1}{2}v_i v_i\right)\right\rangle = \frac{\partial}{\partial t}\left\langle\frac{1}{2}v_i v_i\right\rangle - \frac{1}{V}\int_{A_{\alpha\beta}}\left(\frac{1}{2}v_i v_i\right)\mathbf{w}\cdot\mathbf{n}\,dA \tag{A.6}$$

where $\mathbf{w}$ is the velocity of the interface $A_{\alpha\beta}$, which is zero in the present case. The averaging theorem Eq. (A.4) can be applied to the other terms of the transport equation (Eq. (A.5)). Since the velocity on the interface A_{fs} is zero, Eq. (A.5) reads:

$$\begin{aligned}&\frac{\partial}{\partial t}\left\langle\frac{v_i v_i}{2}\right\rangle + \frac{\partial}{\partial x_j}\left\langle\frac{v_i v_i}{2}v_j\right\rangle \\ &\quad = -\frac{1}{\rho_f}\frac{\partial\langle Pv_j\rangle}{\partial x_j} + \nu_f\frac{\partial}{\partial x_j}\left(\frac{\partial}{\partial x_j}\left\langle\frac{v_i v_i}{2}\right\rangle\right) - \nu_f\left\langle\frac{\partial v_k}{\partial x_j}\frac{\partial v_k}{\partial x_j}\right\rangle\end{aligned} \tag{A.7}$$

Representing the point velocity values as $v_i = \langle v_i\rangle^f + \hat{v}_i$, the mechanical energy is expressed as a sum of a phase averaged contribution and a dispersive mechanical energy term as:

$$\frac{v_i v_i}{2} = \frac{\langle v_i\rangle^f\langle v_i\rangle^f}{2} + \frac{\hat{v}_i\hat{v}_i}{2} + \langle v_i\rangle^f\hat{v}_i \tag{A.8}$$

Evaluation of the different terms of Eq. (A.7) yields an equation that represents the sum of the mechanical energy of the phase averaged flow plus the dispersive mechanical energy. Denoting $K_M = (\langle v_i\rangle^f\langle v_i\rangle^f)/2$ and $k_D = (\hat{v}_i\hat{v}_i)/2$,

$$\begin{aligned}&\frac{\partial\langle K_M\rangle}{\partial t} + \frac{\partial}{\partial x_j}\langle K_M\langle v_j\rangle^f\rangle \\ &\quad - \left[-\frac{1}{\rho_f}\frac{\partial(\langle P\rangle^f\langle v_i\rangle^f)}{\partial x_j} + \nu_f\frac{\partial}{\partial x_j}\left(\frac{\partial}{\partial x_j}\langle K_M\rangle\right)\right. \\ &\quad + \nu_f\left\langle\frac{\partial\langle v_k\rangle^f}{\partial x_j}\frac{\partial\langle v_k\rangle^f}{\partial x_j}\right\rangle + \frac{1}{\rho_f}\frac{\partial}{\partial x_j}\langle-\rho_f\langle v_i\rangle^f\hat{v}_i\hat{v}_j\rangle \\ &\quad \left. - \frac{1}{\rho_f}\langle-\rho_f\hat{v}_i\hat{v}_j\rangle\frac{\partial\langle v_i\rangle^f}{\partial x_j}\right] = -A^*\end{aligned} \tag{A.9}$$

in which A^* is equal to:

$$\begin{aligned}A^* = &\frac{\partial}{\partial t}\langle k_D\rangle + \frac{\partial}{\partial x_j}\langle k_D\langle v_j\rangle^f\rangle \\ &- \left[-\frac{1}{\rho_f}\frac{\partial}{\partial x_j}\langle\hat{P}\hat{v}_j\rangle + \nu_f\frac{\partial}{\partial x_j}\left(\frac{\partial}{\partial x_j}\langle k_D\rangle\right)\right. \\ &\left. -\nu_f\left\langle\frac{\partial\hat{v}_k}{\partial x_j}\frac{\partial\hat{v}_k}{\partial x_j}\right\rangle - \frac{1}{\rho_f}\langle\rho_f\hat{v}_i\hat{v}_j\rangle\frac{\partial\langle v_i\rangle^f}{\partial x_j} - \frac{\partial}{\partial x_j}\left\langle\frac{\hat{v}_i\hat{v}_i}{2}\hat{v}_j\right\rangle\right]\end{aligned} \tag{A.10}$$

Obviously, the LHS of Eq. (A.9) is the phase averaged transport equation for the kinetic energy of the phase averaged velocity, while the RHS of Eq. (A.10) represents the transport equation of the dispersion kinetic energy. The authors point out the analogy with the Reynolds averaging, since all surface integrals vanish because of no-slip conditions, that is familiar to turbulence specialists.

The modelling of the diffusion-like terms may follow the Fick's law gradient type approach. For the diffusion term,

$$-\frac{\partial}{\partial x_j}\left[\frac{1}{\rho_f}\langle\hat{P}\hat{v}_j\rangle-\left\langle\frac{\hat{v}_i\hat{v}_i}{2}\hat{v}_j\right\rangle\right]+\nu_f\frac{\partial}{\partial x_j}\left(\frac{\partial}{\partial x_j}\langle k_D\rangle\right)\simeq D\frac{\partial}{\partial x_j}\left(\frac{\partial}{\partial x_j}\langle k_D\rangle\right) \tag{A.11}$$

A production term is written as:

$$\frac{1}{\rho_f}\langle-\rho_f\hat{v}_i\hat{v}_j\rangle\frac{\partial\langle v_i\rangle^f}{\partial x_j}=P_D \tag{A.12}$$

and a dissipation term is as follows:

$$-\nu_f\left\langle\frac{\partial\hat{v}_k}{\partial x_j}\frac{\partial\hat{v}_k}{\partial x_j}\right\rangle=\Phi \tag{A.13}$$

For the present work, it is supposed that the dispersive energy budget is dominated by production and dissipation. Consequently, the term enclosed in brackets in Eq. (A.10) becomes

$$P_D+\Phi=0 \tag{A.14}$$

One should take into consideration that no time average was considered. Consequently, the derivation of Eq. (A.13) has nothing in common with turbulent kinetic energy. However, both analyses share the concept of averaged velocity (in space or time) that is a pure mathematical one.

References

[1] J.R. Howell, M.J. Hall, J.L. Ellzey, Combustion of hydrocarbon fuels within porous inert media, Prog. Energy Combust. Sci. 22 (1996) 121–145.

[2] D. Trimis, F. Durst, Combustion in a porous medium—Advances and applications, Combust. Sci. Technol. 121 (1996) 153–168.

[3] H.O. Pfannkuch, Contribution à l'étude des deplacements de fluids miscibles dans un milieu poreux, Rev. Inst. Français Pétrole 18 (1963) 215–270.

[4] D.R.F. Harleman, R.R. Rumer, Longitudinal and lateral dispersion in an isotropic porous medium, J. Fluid Mech. 16 (1963) 385–394.

[5] J.J. Fried, M.A. Combarnous, Dispersion in porous media, Adv. Hydrosci. 7 (1971) 169–262.

[6] N.W. Han, J. Bhakia, R.G. Carbonell, Longitudinal and lateral dispersion in packed beds: effect of column length and particle size distribution, AIChE J. 31 (1985) 277–288.

[7] H. Brenner, Dispersion resulting from flow through partially periodic porous media, Philos. Trans. Roy. Soc., London 297 (1980) 81–133.

[8] R.G. Carbonell, S. Whitaker, Dispersion in pulsed systems II—Theoretical developments and passive dispersion in porous media, Chem. Eng. Sci. 38 (1983) 1795–1802.

[9] M. Quintard, S. Whitaker, Transport in ordered and disordered porous media: volume-averaged equations, closure problems, and comparison with experiment, Chem. Eng. Sci. 48 (1993) 2537–2564.

[10] F. Kuwahara, A. Nakayama, H. Koyama, A numerical study of thermal dispersion in porous media, ASME J. Heat Transfer 118 (1996) 756–761.

[11] H.P.A. Souto, C. Moyne, Dispersion in two-dimensional periodic porous media. Part II: Diffusion tensor, Phys. Fluids 9 (1997) 2253–2263.

[12] K.T. Hsiao, S.G. Advani, A theory to describe heat transfer during laminar incompressible flow of a fluid in periodic porous media, Phys. Fluids 11 (1999) 1738–1748.

[13] D.L. Koch, R.G. Cox, H. Brenner, J.F. Brady, The effect of order on dispersion in porous media, J. Fluid Mech. 200 (1989) 173–188.

[14] D.L. Koch, J.F. Brady, Dispersion in fixed beds, J. Fluid Mech. 154 (1985) 399–427.

[15] J. Bear, Dynamics of Fluid in Porous Media, American Elsevier, New York, 1972, pp. 579–664.

[16] D.A. Nield, A. Bejan, Convection in porous media, second ed., Springer-Verlag, New York, 1999, Chapters 2 and 4.

[17] M. Kaviany, Principles of Heat Transfer in Porous Media, second ed., Springer-Verlag, New York, 1995, pp. 157–258.

[18] P. Benz, P. Hütter, A. Schlegel, Radiale Stoffdispersionskoeffizienten in durchströmten keramischen Schäumen, Wärme Stoffübertrag. 29 (1993) 125–127.

[19] C.L. Hackert, J.L. Ellzey, O.A. Ezekoye, M.J. Hall, Transverse dispersion at high Peclet numbers in short porous media, Exper. Fluids 21 (1996) 286–290.

[20] C.P. Lowe, D. Frenkel, Do hydrodynamic dispersion coefficients exist? Phys. Rev. Lett. 77 (22) (1996) 4552–4555.

[21] R.J. Hill, D.L. Koch, Moderate-Reynolds-number flow in a wall-bounded porous medium, J. Fluid Mech. 453 (2002) 315–344.

[22] T. Masuoka, Y. Takatsu, Turbulence model for flow through porous media, Int. J. Heat Mass Transfer 39 (1996) 2803–2809.

[23] B.V. Antohe, J.L. Lage, A general two-equation macroscopic turbulence model for incompressible flow in porous media, Int. J. Heat Mass Transfer 40 (1997) 3013–3024.

[24] V.S. Travkin, L. Catton, Nonlinear effects in multiple regime transport of momentum in longitudinal capillary porous medium morphology, J. Por. Med. 2 (1999) 277–294.

[25] D.A. Nield, Alternative models of turbulence in a porous medium and related matters, ASME J. Fluids Eng. 123 (2001) 928–931.

[26] R.S. Maier, D.M. Kroll, R.S. Bernard, S.E. Howington, J.F. Peters, H.T. Davis, Pore-scale simulation of dispersion, Phys. Fluids 12 (2000) 2065–2079.

[27] K. Vafai, L.C. Tien, Boundary and inertia effects on flow and heat transfer in porous media, Int. J. Heat Mass Transfer 24 (1981) 195–203.

[28] S.V. Patankar, D.B. Spalding, A calculation procedure for heat, mass and momentum transfer in three-dimensional parabolic flows, Int. J. Heat Mass Transfer 15 (1972) 1787–1806.

[29] J.H. Ferziger, M. Perić, Computational Methods for Fluid Dynamics, third rev. ed., Springer-Verlag, Berlin, 2002, pp. 148–151.

[30] K.R. Jolls, T.J. Hanratty, Transition to turbulence for flow through a dumped bed of spheres, Chem. Eng. Sci. 21 (1966) 1185–1190.
[31] A. Dybbs, R.V. Edwards, R.V., A new look at porous media fluid mechanics–Darcy to turbulent, in: J. Bear, M.Y. Corapcioglu (Eds.), Fundamentals of Transport Phenomena in Porous Media, Martinus-Nijhoff Publications, Netherlands, 1984, pp. 199–254.
[32] M.J. Hall, J.P. Hiatt, Measurements of pore scale flows within and exiting ceramic foams, Exper. Fluids 20 (1996) 433–440.
[33] R.C. Hassinger, D.U. von Rosenberg, A mathematical and experimental examination of transverse dispersion coefficients, Soc. Petrol. Eng. J. 243 (1968) 195–204.
[34] A. Bhattacharya, V.V. Calmidi, R.L. Mahajan, Thermophysical properties of high porosity metal foams, Int. J. Heat Mass Transfer 45 (2002) 1017–1031.
[35] B. Alazmi, K. Vafai, Analysis of variants within the porous media transport models, ASME J. Heat Transfer 122 (2000) 303–326.
[36] D.L. Koch, J.F. Brady, The effective diffusivity of fibrous media, AIChE J. 32 (1986) 575–591.
[37] W.G. Gray, A derivation of the equations for multi-phase transport, Chem. Eng. Sci. 30 (1975) 229–233.
[38] V.V. Calmidi, R.L. Mahajan, Forced convection in high porosity metal foam, ASME J. Heat Transfer 122 (2000) 557–565.
[39] H.M. Nepf, Drag, turbulence and diffusion in flow through emergent vegetation, Water Resour. Res. 35 (2) (1999) 479–489.
[40] S. Whitaker, Advances in theory of fluid motion in porous media, Ind. Eng. Chem. 61 (12) (1969) 14–28.
[41] R.B. Bird, W.E. Stewart, E.N. Lightfoot, Transport Phenomena, John Wiley & Sons, Inc., New York, 1960, p. 81.